Briefings in Bioinformatics, 2025, **26(3)**, bbaf229
https://doi.org/10.1093/bib/bbaf229
Case Study

Decoding herbal combination models through systematic strategies: insights from target information and traditional Chinese medicine clinical theory

Mingjuan Wang[1,‡], Xuetong Chen[1,‡,*], Mingxing Liu[1], Huiying Luo[1], Shuangshuang Zhang[1], Jie Guo[2], Jinghui Wang[3], Li Zhou[1], Na Zhang[1], Hongyan Li[2], Chao Wang[4], Liang Li[4], Zhenzhong Wang[4], Haiqing Wang[5], Zihu Guo[5], Yan Li[6], Yonghua Wang[1,2,*]

[1]Key Laboratory of Resource Biology and Biotechnology in Western China, Ministry of Education, School of Life Sciences, Northwest University, No. 229 Taibai North Road, Xi'an 710069, Shaanxi, China
[2]Key Laboratory of Phytomedicinal Resources Utilization, Ministry of Education, Shihezi University, North 4th Road, Shihezi 832000, Xinjiang, China
[3]School of Integrated Chinese and Western Medicine, Anhui University of Chinese Medicine, No. 350 Longzi Lake Road, Hefei 230000, Anhui, China
[4]State Key Laboratory of New-Tech for Chinese Medicine Pharmaceutical Process, Jiangsu Kanion Pharmaceutical Co. Ltd., No. 58 Kangyuan Road, Jiangning Industrial Park, Economic and Technological Development Zone, Lianyungang 222002, Jiangsu, China
[5]Life Sciences Research Department, Collaborative Innovation Center of Qiyao in Mt. Qinling, No. 3, East Section of Gao Gan Qu Road, Yangling 712100, Shaanxi, China
[6]Key Laboratory of Industrial Ecology and Environmental Engineering, Faculty of Chemical, Environmental and Biological Science and Technology, Dalian University of Technology, No. 2 Lingong Road, Ganjingzi District, Dalian 116000, Liaoning, China

*Corresponding authors. Xuetong Chen, Key Laboratory of Resource Biology and Biotechnology in Western China, Ministry of Education, School of Life Sciences, Northwest University, No. 229 Taibai North Road, Xi'an 710069, Shaanxi, China. E-mail: xuetongchen@nwu.edu.cn; Yonghua Wang, Key Laboratory of Resource Biology and Biotechnology in Western China, Ministry of Education, School of Life Sciences, Northwest University, No. 229 Taibai North Road, Xi'an 710069, Shaanxi, China. E-mail: yhwang@nwu.edu.cn

‡Mingjuan Wang and Xuetong Chen contributed equally to this work and should be considered co-first authors.

Xuetong Chen and Yonghua Wang should be considered as co-corresponding authors.

Abstract

Traditional Chinese medicine (TCM) utilizes intricate herbal formulations that exemplify the principles of compatibility and synergy. However, the rapid proliferation of herbal data has resulted in redundant information, complicating the understanding of their potential mechanisms. To address this issue, we first established a comprehensive database that encompasses 992 herbs, 18 681 molecules, and 2168 targets. Consequently, we implemented a multi-network strategy based on a core information screening method to elucidate the highly intertwined relationships among the targets of various herbs and to refine herbal target information. Within a non-redundant network framework, separation and overlap analysis demonstrated that the networking of herbs preserves essential clinical information, including their properties, meridians, and therapeutic classifications. Furthermore, two notable trends emerged from the statistical analyses of classical TCM formulas: the separation of herbs and the overlap between herbs and diseases. This phenomenon is termed the herbal combination model (HCM), validated through statistical analyses of two representative case studies: the common cold and rheumatoid arthritis. Additionally, in vivo and in vitro experiments with the new formula YanChuanQin (YanHuSuo—Corydalis Rhizoma, ChuanWu—Aconiti Radix, and QinJiao—Gentianae Macrophyllae Radix) for acute gouty arthritis further support the HCM. Overall, this computational method provides a systematic network strategy for exploring herbal combinations in complex and poorly understood diseases from a non-redundant perspective.

Keywords: Traditional Chinese Medicine; non-redundant network; clinical network representation; herbal combination model; acute gouty arthritis

Introduction

As the core carrier of Traditional Chinese Medicine (TCM) clinical practice, TCM formulas have developed a unique compatibility system after thousands of years of clinical experience and theoretical refinement. This complex compatibility theory places a greater emphasis on the balance between the individual and their environment, as well as the interconnections among various physiological systems [1]. The holistic approach inherent in TCM, which achieves the comprehensive regulation of complex diseases through the synergistic effects of multiple herbs, closely aligns with the principles of modern systems biology [2]. Nevertheless, the intricate nature of TCM—characterized by its multi-molecular and multi-target properties—along with the "big bang trend" of herbal combinations, presents challenges in discerning the principles of compatibility in TCM when relying solely on traditional practice [3]. Therefore, this complexity hinders a clear understanding of the mechanisms and principles underlying TCM formulas.

Received: January 23, 2025. **Revised:** April 12, 2025. **Accepted:** April 28, 2025

The vast accumulated clinical and experimental knowledge of TCM formulas over the centuries (especially in recent times) requires exploration using more in-depth and systematic approaches through modern biological and computational methods [4]. Recently, network pharmacology has emerged as a promising approach for studying TCM [5]. This approach enables researchers to visualize and analyze the complex actions of herbal molecules and their targets, thereby enhancing the understanding of the mechanisms underlying herbal combinations. And network analysis recognizes the synergistic efficacy of a TCM formula by parsing its entire set of molecules and targets, rather than focusing on individual molecule [6]. However, the multi-molecule and multi-target characteristics of herbal systems present the challenge of information redundancy for network analysis [7]. The overlap of molecules and targets among different herbs obscures the unique contribution of each herb within the formulation, particularly in the context of complex prescriptions. Moreover, the consistency validation between the network and the clinical attributes and biological properties of the herbs is often overlooked during the TCM networking process. This neglect can significantly impact the applicability and accuracy of network analysis in real therapeutic scenarios. Therefore, refining network models to minimize redundancy and enhance clarity in interactions is crucial for accurately representing the efficacy of herbal combinations.

Here, we utilized network separation and overlap strategies to systematically explore the networked processes and compatibility principles of herbal combinations in TCM. First, we developed a core target screening method to obtain the core targets of herbs, thus effectively filtering the high overlap and low-frequency target information among herbs and alleviating the information redundancy challenges posed by the multi-molecule and multi-target nature of TCM. The efficacy of the non-redundant TCM network was validated through an analysis of herb–herb relationships, herbal clinical information, classic herbal pairs, and classic herbal formulas. This process culminated in the development of the herbal combination model (HCM), which encapsulates the interactions and synergies among herbs. The HCM was validated with the new formula YanChuanQin, serving as a practical case study. Ultimately, this research aims to advance the theoretical framework of herbal formulations in TCM while providing a foundation for developing more effective, scientifically validated herbal combinations that integrate traditional practices with network topology insights (Fig. 1).

Materials and methods

Herbal library and its annotation information

We established a comprehensive TCM library based on the Chinese Pharmacopeia, integrating data from the Traditional Chinese Medicine Systems Pharmacology Database and Analysis Platform (TCMSP) [8], Chinese Traditional Medicine Database (TCMID) [9], and SuperTCM [10] databases. This library includes 992 herbs and 18 681 molecules. Additionally, we identified 712 classic herbal pairs and 3560 classic formulas corresponding to these herbs from the TCMID (https://cintmed.cintcm.cn/cintmed). All entries underwent manual verification to standardize and ensure the accuracy of the information.

Next, we utilized the systematic drug targeting tool [11], the weighted integrated similarity tool [12], and the ChEMBL database (Version 33) [13] to integrate the potential targets for the 18 681 molecules. This process identified 2168 potential targets, which were mapped to the UniProt database (https://www.uniprot.org/) for normalization. We also collected disease gene annotation data from the DISEASES database [14], which compiles disease–gene associations from text mining, literature curation, cancer mutation data, and genome-wide association studies. To address multi-level disease classification, when specific disease data were unavailable in DISEASES, we expanded our search for disease-associated genes to include DrugBank [15], DisGeNET [16], GeneCards [17], and OMIM [18]. This study focused on three diseases: common cold disorder, rheumatoid arthritis (RA), and acute gouty arthritis (AGA).

Calculation of core targets of herbal medicine

To identify the core targets of each herb, we employed a random molecule library consisting of all 18 826 molecules from the herbal medicine database (Supplementary Fig. S1a). Firstly, we defined the weight of an herbal target as the number of herbal molecules that interact with it. Briefly, the core evaluation process of herbal targets is divided into three steps: (1) a random herb with an equivalent number of molecules from the library was created to evaluate the target weights for this herb; (2) this randomization process was repeated 1000 times [19] to generate a random distribution of target weights for each herb; (3) the random mean and standard deviation of each target's weight were calculated to assess the significance of the actual herbal targets via the Z-score Equation (1):

$$Z\ \text{score}_{T_m}^{H_n} = \left(\text{Weight}_{T_m}^{H_n} - \text{Weight}_{T_m^R}^{\text{Mean}}\right) \Big/ \text{Weight}_{T_m^R}^{SD} \tag{1}$$

where $\text{Weight}_{T_m}^{H_n}$ is the weight value of the mth target of the nth herb, $\text{Weight}_{T_m^R}^{\text{Mean}}$ and $\text{Weight}_{T_m^R}^{SD}$ are the mean and standard deviation of the random distribution for that target, and $Z\ \text{score}_{T_m}^{H_n}$ is the core assessment value of that target.

Network calculation of target sets of herbal medicines

To evaluate the overlap between different herbal target sets, we applied Jaccard similarity (JS) (2) and cosine similarity (CS) (3) methods to assess the similarity between pairs of herbs:

$$JS_{H_A}^{H_B} = \left|TS_{H_A} \cap TS_{H_B}\right| / \left|TS_{H_A} \cup TS_{H_B}\right| \tag{2}$$

where TS_{H_A} and TS_{H_B} are the target sets for herbs A and B, respectively. $\left|TS_{H_A} \cap TS_{H_B}\right|$ and $\left|TS_{H_A} \cup TS_{H_B}\right|$ are the size of the intersection targets and union targets of two herbs. A JS value of 1 signifies identical target sets, while a value of 0 indicates no overlap.

$$V_{H_A} = \left(T_1^A, T_2^A, T_3^A, \cdots, T_n^A\right)$$

$$V_{H_B} = \left(T_1^B, T_2^B, T_3^B, \cdots, T_n^B\right)$$

$$CS_{H_A}^{H_B} = \left(V_{H_A} \cdot V_{H_B}\right) / \left(\left\|V_{H_A}\right\| \times \left\|V_{H_B}\right\|\right) \tag{3}$$

where V_{H_A} and V_{H_B} are weight vectors from the target sets, $V_{H_A} \cdot V_{H_B}$ denotes the dot products, and $\left\|V_{H_A}\right\|$ and $\left\|V_{H_B}\right\|$ represent their Euclidean norms. The CS value ranges from −1 to 1; a value of 1 indicates coincident vectors, while −1 indicates oppositional vectors.

The High-quality INTeractomes (v202402) [20] database was used to construct a protein–protein interaction (PPI) network (16 677 proteins and 243 603 interactions). And the network topological properties between herbal targets were evaluated based on this PPI network, including distance and separation properties (Supplementary Fig. S1b). The distance between herbs was

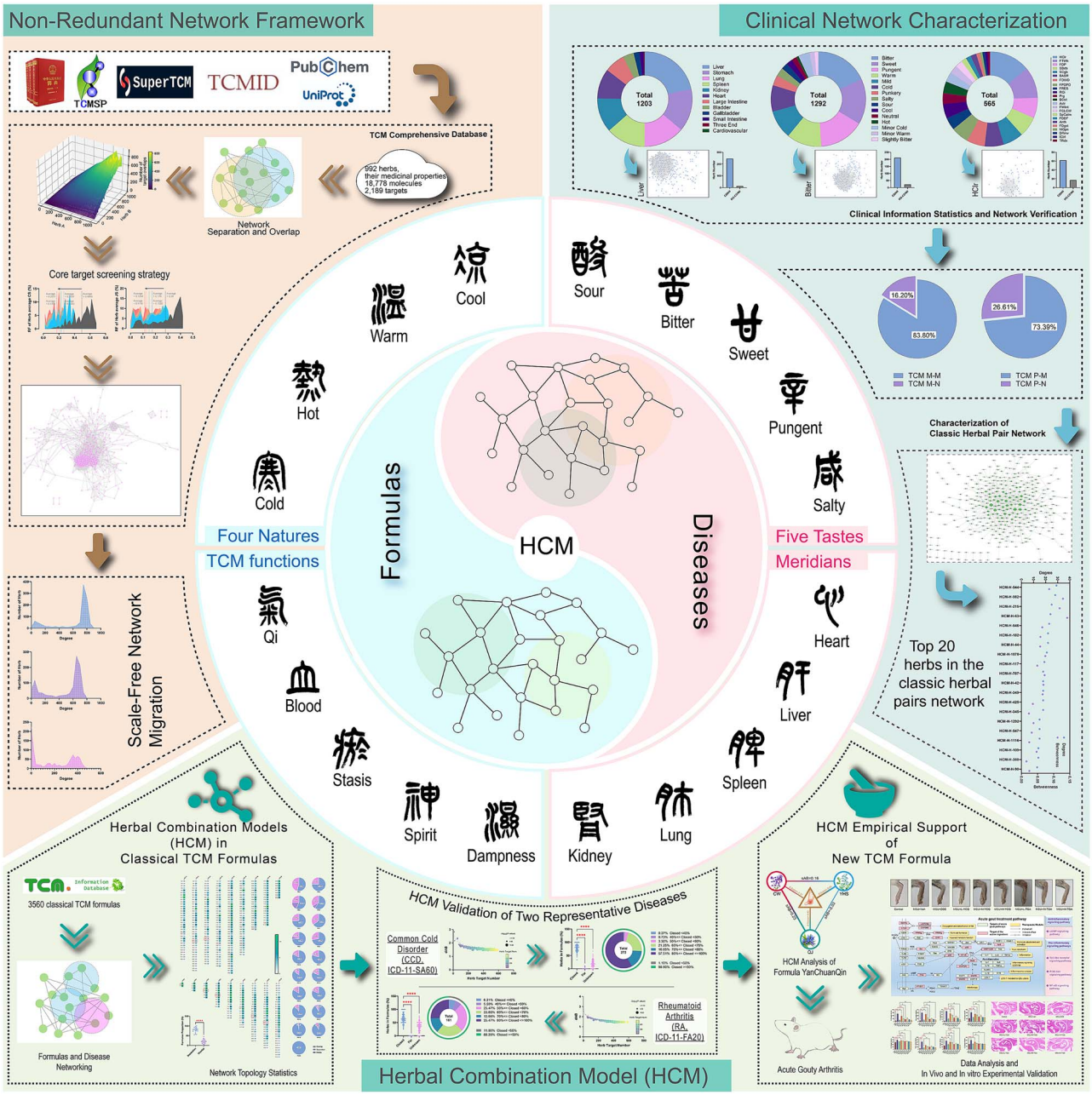

Figure 1. Construction and verification of HCM based on non-redundant network modeling.

evaluated using the average shortest path length (closest) [19, 21] Equation (4):

$$d_{H_A}^{H_B} = \left(\sum_{T_A \in TS_{H_A}} \min_{T_B \in TS_{H_B}} d(T_A, T_B) + \sum_{T_B \in TS_{H_B}} \min_{T_A \in TS_{H_A}} d(T_B, T_A) \right) / \left(\|TS_{H_A}\| + \|TS_{H_B}\| \right) \quad (4)$$

where TS_{H_A} and TS_{H_B} are the herbal target sets of herbs A and B, respectively. T_A and T_B are the target in the target sets. $d(T_A, T_B)$ indicates the shortest distance between two targets within the PPI network, while $d_{H_A}^{H_B}$ signifies the average shortest distance between the two herbal target sets, labeled as distance between herb A and herb B (dAB).

The separation between herbs was assessed using the network proximity Equation (5):

$$s_{H_A}^{H_B} = d_{H_A}^{H_B} - \left(d_{H_A}^{H_A} + d_{H_B}^{H_B} \right) / 2 \quad (5)$$

where $d_{H_A}^{H_A}$, $d_{H_B}^{H_B}$, and $d_{H_A}^{H_B}$ denote the average shortest distances between targets within herbs A and B, and between the two herbs, respectively. And $s_{H_A}^{H_B}$ was used to evaluate the separation and overlap trends between the target sets of herbs A and B, labeled as separation between herb A and herb B (sAB). A threshold of −0.6162 was established for defining separation and overlap; $s_{H_A}^{H_B} \geq -0.6162$ indicates separation, while $s_{H_A}^{H_B} < -0.6162$ suggests overlap.

The significance of the distance between the herb and the disease was assessed by comparing it to a random distribution

Equation (6), where the random process is similar to the core target method:

$$\text{Zscore}_H^D = \left(d_H^D - d_{R_H^D}^{\text{Mean}}\right) \Big/ d_{R_H^D}^{SD} \quad (6)$$

where d_H^D represents the average shortest distance between the herb and disease, $d_{R_H^D}^{\text{Mean}}$ denotes the mean of the random distribution, $d_{R_H^D}^{SD}$ indicates the standard deviation of that distribution, and Zscore_H^D provides a consistent measure of network proximity between the herb and the disease.

Systemic pharmacology analysis of YanChuanQin formula

The new herbal formula YanChuanQin (YCQ, Chinese Patent Number: CN 202411051001.9) includes Corydalis Rhizoma (YanHuSuo [YHS], HCM-H-1356), Aconiti Radix (ChuanWu [CW], HCM-H-136), and Gentianae Macrophyllae Radix (QinJiao [QJ], HCM-H-951). This formulation has the effects of dispelling wind and dampness, promoting blood circulation and relieving pain, and is used to treat AGA [22, 23]. We calculated the pharmacokinetic properties of 189 molecules in YCQ, including Lipinski's rule of five (molecular weight [MW] ≤ 600 [24], Number of Donor Atoms for H-bonds ≤ 5, Number of Acceptor Atoms for H-bonds ≤ 10, Ghose-Crippen octanol–water partition coefficient ≤ 5, and Number of Rotatable Bonds ≤ 10) and Drug-Likeness (≥0.18), primarily sourced from the TCMSP, to identify 111 potential active molecules. The structural classification of these molecules included flavonoids, alkaloids, anthraquinones, phenylpropanoids, glycosides, steroids, and terpenoids. The potential targets of these molecules were identified from our herbal medicine library and compared to those associated with AGA, resulting in 45 common targets.

The BioGPS database [25] was used to assess the expression of 45 intersection targets across various tissues. We also performed gene ontology (GO) and Kyoto Encyclopedia of Genes and Genomes (KEGG) pathway enrichment analyses using the Metascape server [26]. All KEGG-enriched pathways were manually integrated to create a comprehensive pathway diagram for YCQ's treatment of AGA. The networks representing the relationships among various elements (molecules, targets, pathways, etc.) were constructed by Cytoscape (version 3.9) [27]. In the Component–Component (C–C) network, connections were established based on a Tanimoto coefficient value of 0.85 or higher, assessed through molecular descriptors derived from Dragon (http://www.talete.mi.it/index.htm). The C–C network formed four distinct clusters using the MCODE plugin (https://mcode.readthedocs.io/en/latest).

Experimental verification of the YanChuanQin formula

All animal care and experimental procedures involving YCQ, which includes YHS, CW, QJ, and their key constituents (tetrahydropalmatine, gentiopicroside, and aconitine—collectively referred to as TGA), were approved by the Ethical Review Committee for Laboratory Animal Management and Welfare at Northwest A&F University (Permission Number: XN2024–0317). The studies adhered strictly to the Guide for the Care and Use of Laboratory Animals. Male BALB/c mice (8 weeks, 23 ± 2 g) were obtained from Hunan Slake Jinda Laboratory Animal Co., Ltd. Experiments were conducted under standard conditions: a 12-h light–dark cycle, temperature of 24 ± 2°C, and humidity of 55 ± 5%. Mice had access to food and water ad libitum and were housed in groups of five, with a 1-week acclimatization period before the experiments.

A total of 90 mice were randomly assigned to nine groups: a control group, a model group, a positive drug group (diclofenac diethylamine emulgel, DDE), and six treatment groups (L-YCQ, M-YCQ, H-YCQ, L-TGA, M-TGA, and H-TGA, where L, M, and H represent low, medium, and high doses, respectively). After anesthetization, the right hind ankle of each mouse was shaved, and 20 μl of monosodium urate (MSU) crystals (0.5 mg) (Merck, Germany, cat: 1198-77-2) suspended in sterile PBS (Cytiva, China, cat: SH30256.01) was injected into the ankle joints. The control group received an injection of 20 μl of sterile PBS. The establishment of the AGA model was confirmed by observing significant swelling and thermal hyperalgesia in the ankle joints 2 h post-injection of MSU crystals.

The drug ratios for each group were as follows: (1) The matrix for YCQ and TGA comprised 1% Carbomer 980F (Beijing Solepol Science and Technology Co., Ltd., China), 4% 1,2-propanediol (Tianjin Tianli Chemical Reagent Co., Ltd., China), and 4% lauric acid azelnidinone (Xi'an Mugo Biotechnology Co., Ltd., China), with a drug-to-matrix ratio of 0.25% (g/g); (2) L-YCQ contained YHS extract (4.354 g, cat: MG-2023092804), CW extract (261.252 mg, cat: MG-2023100501), and QJ extract (2.177 g, cat: MG-2023091602) from Xi'an Mugo Biotechnology Co., Ltd., China, with M-YCQ and H-YCQ representing two and four times the concentration of L-YCQ, respectively; (3) L-TGA included tetrahydropalmatine (21.771 mg, Shanghai Aladdin Biochemical Technology Co., Ltd., China, cat: T101542), gentiopicroside (130.626 mg, Shanghai Yuanye Biotechnology Co., Ltd., China, cat: S25448), and aconitine (0.653 mg, Chengdu Manster Biotechnology Co., Ltd., China, cat: A0196), with M-TGA and H-TGA being two and four times the concentration of L-TGA, respectively; (4) DDE was sourced from Beijing Novartis Pharma Co., Ltd., China (cat: 2079595). The drugs were administered 1 h before the MSU injection and subsequently at 4, 9, 13, 23, and 47 h post-injection. One hour after the final dose, the mice were euthanized, and serum and tissues were collected for analysis.

The ankle swelling index (ASI) and thermal withdrawal latency (TWL) of the mice were measured using a toe volumetric instrument (Beijing Jinyangwanda Technology Co., Ltd., China) and a plantar thermal testing instrument (Nanjing Calvin Biotechnology Co., Ltd., China), respectively. For histological analysis, the ankle joints were fixed in 4% paraformaldehyde (Biosharp, Canada, cat: BL539A), decalcified using Ethylenediaminetetraacetic acid (EDTA) (Shaanxi Zhonghui Hecai Biomedical Science and Technology Co., Ltd., China, cat: PI014), and embedded in paraffin wax (Biosharp, Canada, cat: BL954A). Paraffin sections were stained with hematoxylin and eosin (Beijing Solarbio Science & Technology Co., Ltd., China, cat: G1120) for morphological evaluation under a 5× objective lens. The number of inflammatory cells in each observation field was counted blindly and normalized to the control group. The levels of IL-1β, IL-6, TNF-α, and IL-18 in serum and ankle tissues were measured using enzyme-linked immunosorbent assay (ELISA) procedures (Shanghai Xinyu Biotechnology Co., Ltd., China). All tests were conducted by an experimenter blinded to the experimental conditions.

Data and statistical analysis

All data were included in the analysis and presentation. Only studies with a minimum group size of $n = 3$ were statistically analyzed, where the group size is defined as the number of independent values utilized for analysis. A t-test was employed

to assess differences between two groups, while the one-way analysis of variance was used for comparisons among multiple groups. A *P*-value of <.05 was considered statistically significant.

Results

Network construction of complex herbal medicine systems

To investigate the adaptability and compatibility of network analysis within the intricate framework of TCM, we first established a comprehensive TCM annotation comprised 992 herbs along with their medicinal properties, 18 681 molecules, and 2168 targets (Supplementary Table S1). Next, we employed the network separation and overlap algorithm strategy (see Methods) to connect the biological characteristics (targets) of various herbs and analyze their pharmacological differences. Notably, we observed a significant aggregation effect among the herbs within the network, indicated by an average dAB value (Equation (4)) of 1.1381 (±0.6571) and an average sAB value (Equation (5)) of −0.4519 (±0.4733) (Fig. 2a and b). Furthermore, 78.53% of the sAB values among herbal pairs were below 0 (Fig. 2b), complicating the differentiation of herbs. In-depth analysis revealed that the partial overlap of herbal molecules, combined with their multi-target nature (Supplementary Fig. S2a–g), contributes to the characteristics of herbal targets, including a high average number of targets (396.90) and a substantial overlap rate among herbs (75.24%) (Fig. 2c–f). These findings suggest that screening and refining herbal targets may reduce information interference during the networking process of TCM.

Consequently, we developed a random herbal strategy for core target screening. Specifically, a random herb distribution was constructed for each herb, and the significance of herbal target weights (Equation (1)) was calculated to identify core targets relevant to each herb (see Methods). Based on these core targets, herbs exhibited significant reductions in similarity, as indicated by JS (Equation (2)) and CS (Equation (3)), along with the numbers of intersection and union targets compared to unprocessed herbs (Fig. 2g–j). This trend was consistent across the four selected thresholds for core target screening. Moreover, the average distributions of JS and CS for each herb clarified the screening effects of these thresholds (Fig. 2k and l). As screening thresholds increased, the number of core targets among the herbs consistently decreased (Supplementary Fig. S3a–d). Comparisons of core target proportions across different thresholds showed only a minor difference (−7.89%) between *P*-values of <.01 and <.05. In contrast, substantial differences were noted between the other two thresholds and *P*-value < .05, with average differences of −16.17% and −22.48%, respectively (Supplementary Fig. S3e). The average proportion of core targets at the threshold of *P*-value < .01 was found to be 61.16% (Fig. 2m). Furthermore, a comparison of the distribution of core and non-core targets under this condition indicated that core targets maintained a significant amount of common information in the herbs (Supplementary Fig. S4a–k). Therefore, considering the effectiveness of core target screening and the potential information loss regarding herbal targets, we selected a *P*-value < .01 as the threshold for core target screening of each herb.

Next, we further assessed the impact of the core target strategy on the network representation of herbs. Comparing the sAB and dAB values for herb pairs based on core targets versus original targets revealed that over 90% of herb pairs showed increases in both sAB and dAB values (Fig. 3a). This finding suggests that the core target strategy effectively enhances the separation of herbs within the network, highlighting their unique characteristics. Subsequently, we selected three thresholds (0, −0.1752, −0.6162) to define the network's topological features based on experience and data distribution features (mean and deviation), allowing us to construct the corresponding herb-herb interaction network (Supplementary Fig. S4l). Notably, the thresholds of 0 and −0.1752 could not dissociate the strong clustering properties of the network based on the topology analysis (Fig. 3b–e and Supplementary Fig. S4m). In contrast, the network with a threshold of −0.6162 displayed characteristics of a scale-free network [28], suggesting that it encompasses specific biological information (Fig. 3f and g). Furthermore, most of the herbs in this network were interconnected, and only 30 herbs remained completely independent (Supplementary Fig. S4n). Collectively, these results support the notion that the network representation of herbs, utilizing the core target strategy, is biologically plausible and serves as a non-redundant network framework.

Network adaptation and validation based on clinical attributes of herbs

To examine the alignment of the network representation of herbs with established clinical knowledge, we compiled herbal essential clinical attributes, including properties, meridian affiliations, and therapeutic classifications (Supplementary Table S2). These herbs predominantly target organs such as the liver, stomach, lungs, and spleen, which are common sites for various diseases (Fig. 4a). Notably, the liver and stomach play crucial roles in the absorption of orally administered medications [29, 30]. The properties (e.g. bitter, sweet, spicy) and functions (e.g. clearing heat, tonifying deficiency, resolving phlegm) of most herbs demonstrated a strong consistency with the characteristics of natural plants and their clinical applications (Fig. 4b and c). Further analysis indicated that herbs with similar properties and meridian affiliations are more likely to establish overlapping connections in the network (Fig. 4d and e). A similar trend was observed among herbs with identical functions (Fig. 4f). These findings confirm that the network representation of herbs is not only a method for displaying information but also encapsulates substantial clinical insights.

Network verification of synergistic effects in classic herbal pairs

It is intriguing to investigate whether the network representation of herbs can be extended to combinations of herbs. Statistical analysis of the properties and meridian affiliations of 712 classic herbal pairs revealed significant overlaps in both dimensions, with property and meridian overlap rates of 83.8% and 73.39%, respectively (Fig. 5a–d and Supplementary Table S3). Furthermore, the distribution of sAB values indicates that these herbal combinations tend to exhibit network separation (61.66%) while still functioning synergistically. Notably, some overlapping herbs, concerning their properties and meridian affiliations, coexist within the network to exert synergistic effects (Fig. 5e and f). This finding aligns with the traditional principles of herbal compatibility in TCM, encompassing the concepts of "mutual reinforcement" and "mutual assistance" [31, 32]. Through an analysis of degree and betweenness centrality within network of classic herbal pairs, we identified the most frequently used herbs. The top five herbs are Coptidis Rhizoma (HCM-H-544), Ginseng (HCM-H-982), Angelicae Sinensis Radix (HCM-H-215), Pinelliae Rhizoma (HCM-H-63), and Astragali Radix (HCM-H-546) (Fig. 5g and h). These herbs are often preferred in clinical applications due to their diverse effects, including tonifying Qi, tonifying blood, activating blood, drying

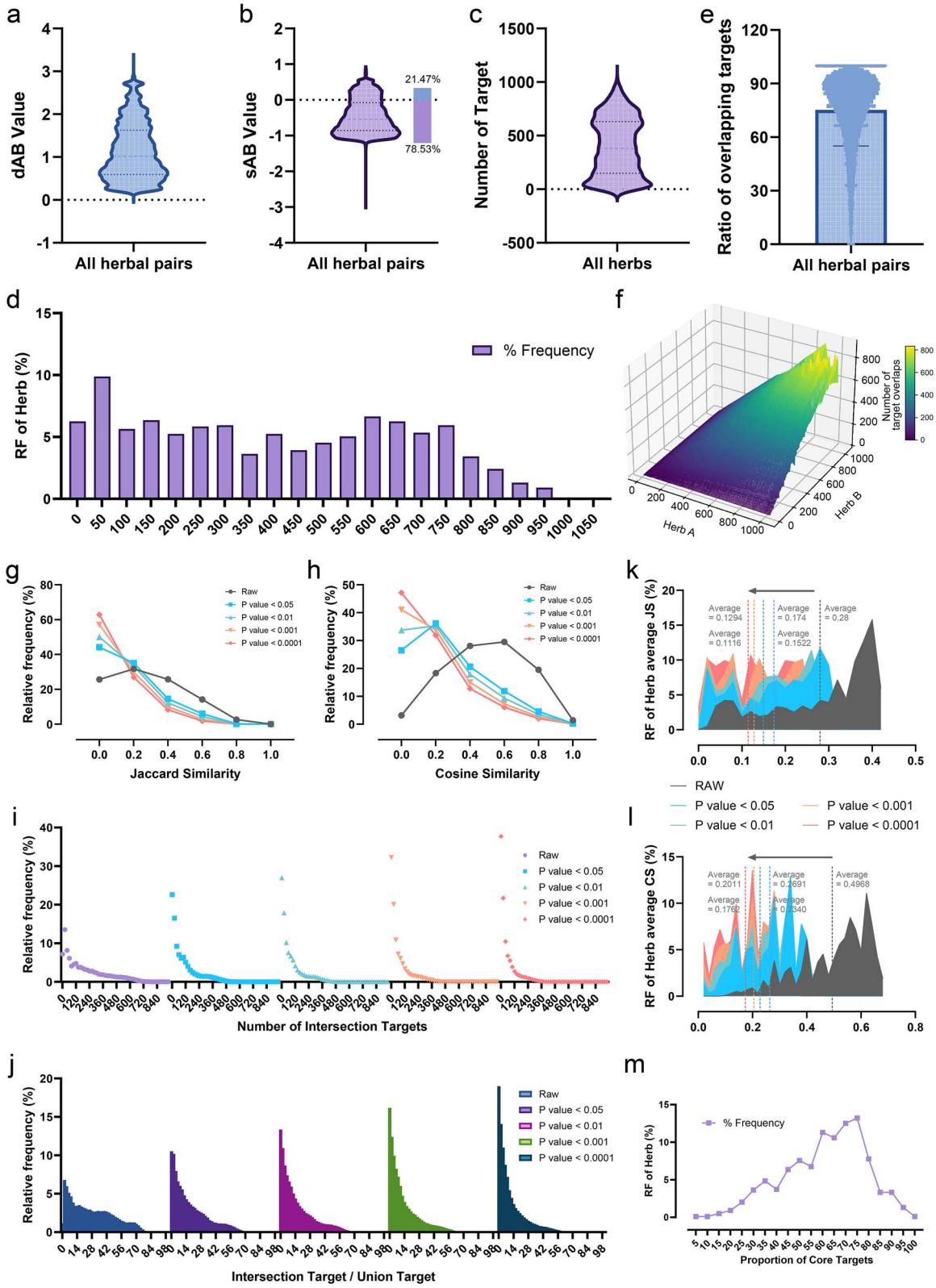

Figure 2. Network analysis and core target screening in traditional Chinese medicine (TCM). (a and b) The violin plot of dAB and sAB values for each herbal pair, while the bar plot illustrates the proportion of herbal pairs with sAB values above or below zero. (c and d) The violin plot and histogram plot of the number of targets associated with each herb. (e) The scatter plot with the target overlap rate bar across all herbal pairs. (f) The 3D surface plot of the number of overlapping targets among all herbal pairs. (g and h) The histogram plot of JS and CS values for all herbal pairs, based on raw target data and core target data with four screening thresholds. (i and j) The histogram plot of the number of intersection targets and the ratio of intersection targets to union targets for all herbal pairs, based on raw target data and core target data with four screening thresholds. (k and l) The histogram plot of the herbal average JS and CS values for all herbal pairs, based on raw target data and core target data with four screening thresholds. (m) The histogram plot of the proportion of core targets of each herb, utilizing a core target screening threshold of 0.01.

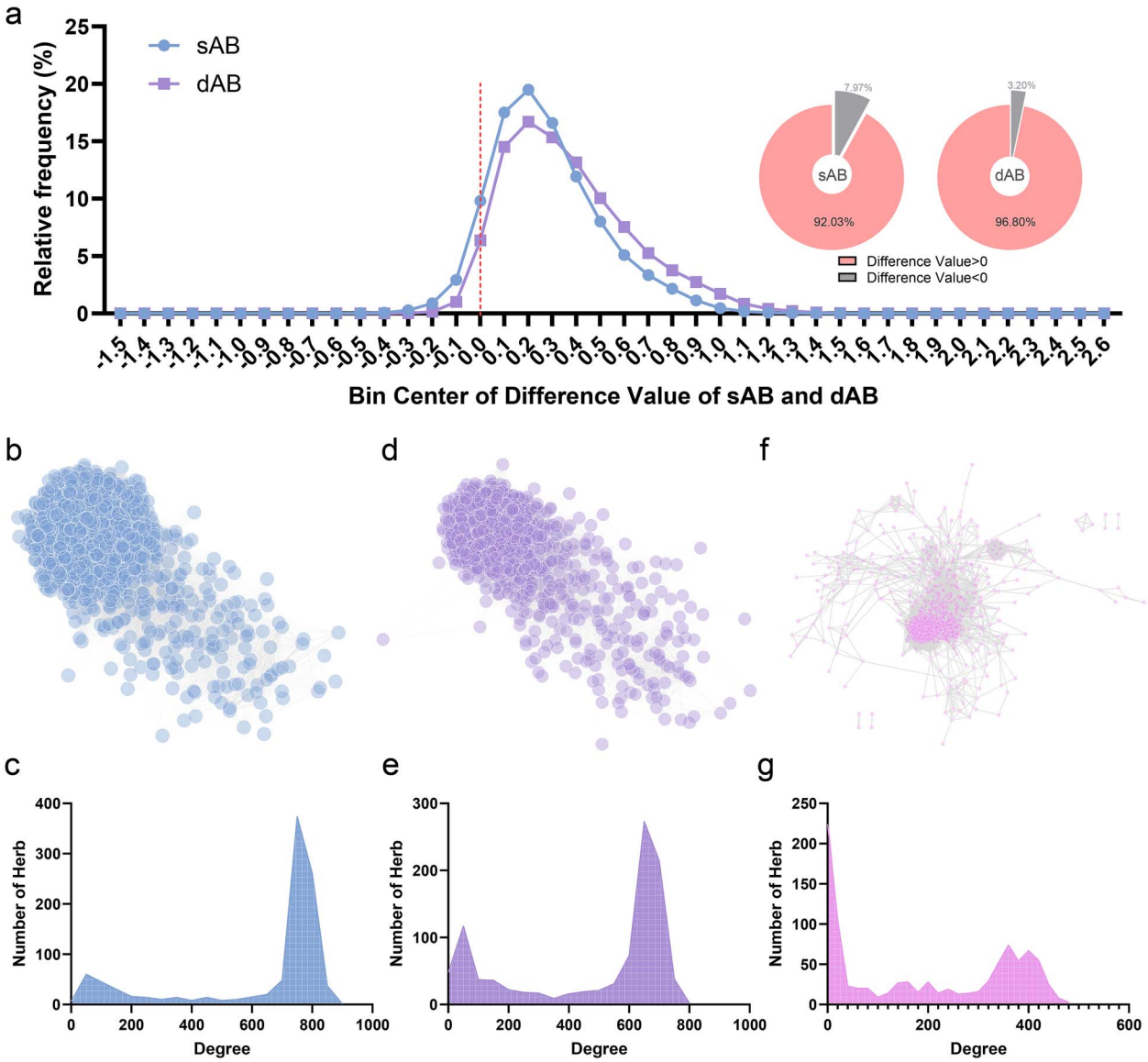

Figure 3. Impact of core target strategy on herbal network representation. (a) The histogram plot of the difference value of distance dAB and sAB for each herbal pair, while the two donut plots represent the proportions of difference values for sAB and dAB that are >0 and <0. (b–g) The network plot of herb–herb relationships along with their corresponding histogram plot of herbal degree values, based on different network separation overlap thresholds: 0 (b–c), −0.1752 (d and e), and −0.6162 (f and g).

dampness, resolving phlegm, and clearing heat [33–37]. They play significant roles in various physiological systems, including the nervous, cardiovascular, endocrine, digestive, reproductive, respiratory, and immune system [36, 38–42]. Overall, the herbal network representation not only encompasses the network footprints of each herb but also serves as a reliable measure of herb–herb relationships, thereby revealing potential synergistic information within herbal pairs.

Network deconstruction of herbal combination models in classical traditional Chinese medicine formulas

Next, we present a network analysis of herbs within the context of 3560 classic TCM formulas to elucidate the underlying principles of herbal formulation (Supplementary Table S4). Interestingly, the top 20 most frequently used herbs distinguished themselves clearly from others within these formulas based on their average sAB values (Fig. 6a and Supplementary Table S5). Notably, licorice (HCM-H-349), the most commonly used herb in 1356 formulas, is frequently utilized in clinical practice to "harmonize various medicines" [43], thereby enhancing their synergistic effects and overall therapeutic efficacy [44]. In classic formulas with varying quantities of herbs, we observed a pronounced phenomenon of network separation as the number of herbs increased (Supplementary Fig. S5a and b). Further proportion analysis of the overlap and separation among herbs in the formulas indicated that as the number of herbs increased, these herbs tended to form topologically distinct combinations (Fig. 6b and c and Supplementary Table S6). Notably, the number of formulas showing a tendency toward topological separation was significantly higher than those exhibiting topological overlap (Fig. 6d). These findings suggest that herbs are frequently combined in a separate network mode, targeting distinct sets of biological targets to exert synergistic

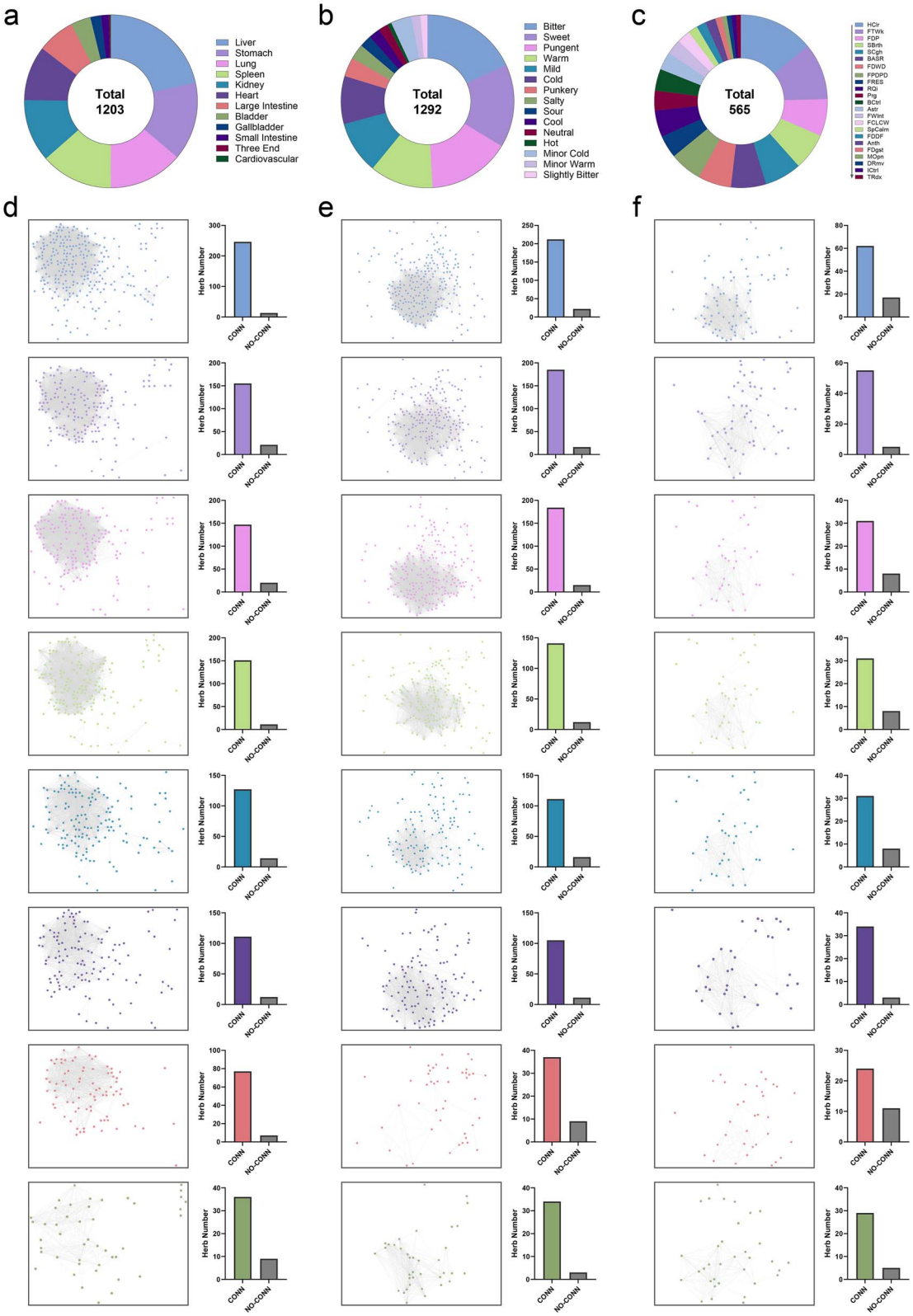

Figure 4. Alignment analysis of herbal network representation with established clinical attributes. (a—c) The donut plots of the proportions of herbal clinical attributes: meridians (a), properties (b), and therapeutic classifications (c). (d–f) The subnetwork plot of the top eight individual clinical attributes (d—meridians, e—properties, and f—therapeutic classifications) of herbs from the sAB-based herb–herb network, while the corresponding bar plot shows the number of connected and unconnected herbs within the subnetwork. The abbreviations for the therapeutic classifications are as follows: Heat clearance, for tonifying weakness, for dissolving phlegm, soothing breathing, stopping cough, blood activation and stasis removal, for promoting diuresis and penetrating dampness, for dispelling wind-dampness, for relieving exterior syndrome, regulation of Qi, purging, bleeding control, Astriction, for warming interior, for calming liver and containing wind, spirit calming, for dissolving dampness by flavors, anthelmintic, food digestion, mind opening, dampness removal, itching control, and toxication reduction.

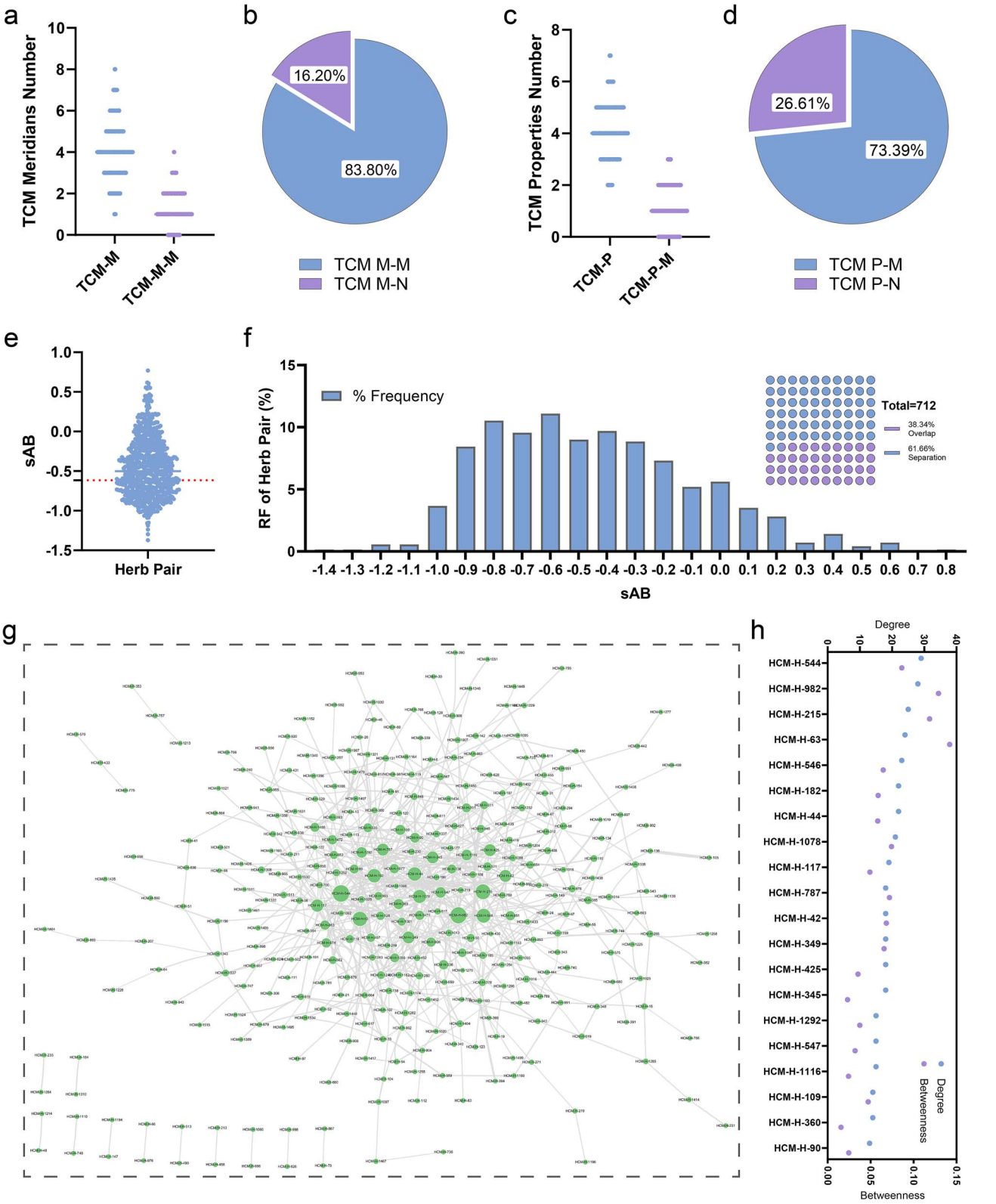

Figure 5. Network module location of classic herbal pairs. (a) The scatter plot of the number of the meridians and their duplicate meridians in each classic herbal pair, while the traditional Chinese medicine meridians stands for meridians in herb pairs, and traditional Chinese medicine meridians-multiple meridians stands for duplicate meridians in herb pairs. (b) The pie plot of the proportions of herbal pairs with and without duplicate meridians, while the traditional Chinese medicine meridians-no multiple meridians stands for no duplicate meridians in herb pairs. (c) The scatter plot of the number of the properties and their duplicate properties in each classic herbal pair, while the traditional Chinese medicine properties stands for properties in herb pairs, and traditional Chinese medicine properties-multiple properties stands for duplicate properties in herb pairs. (d) The pie plot of the proportions of herbal pairs with and without duplicate properties, while the traditional Chinese medicine properties-no multiple properties stands for no duplicate properties in herb pairs. (e and f) The scatter plot and histogram plot of the sAB values for each classic herbal pair, while the dot plot shows the proportions of overlapping and separate herbal pairs. (g) The network plot of classic herbal pairs is based on sAB values. (h) The interleaved scatter plot of the degree and betweenness values of the top 20 herbs in the classic herbal pairs network.

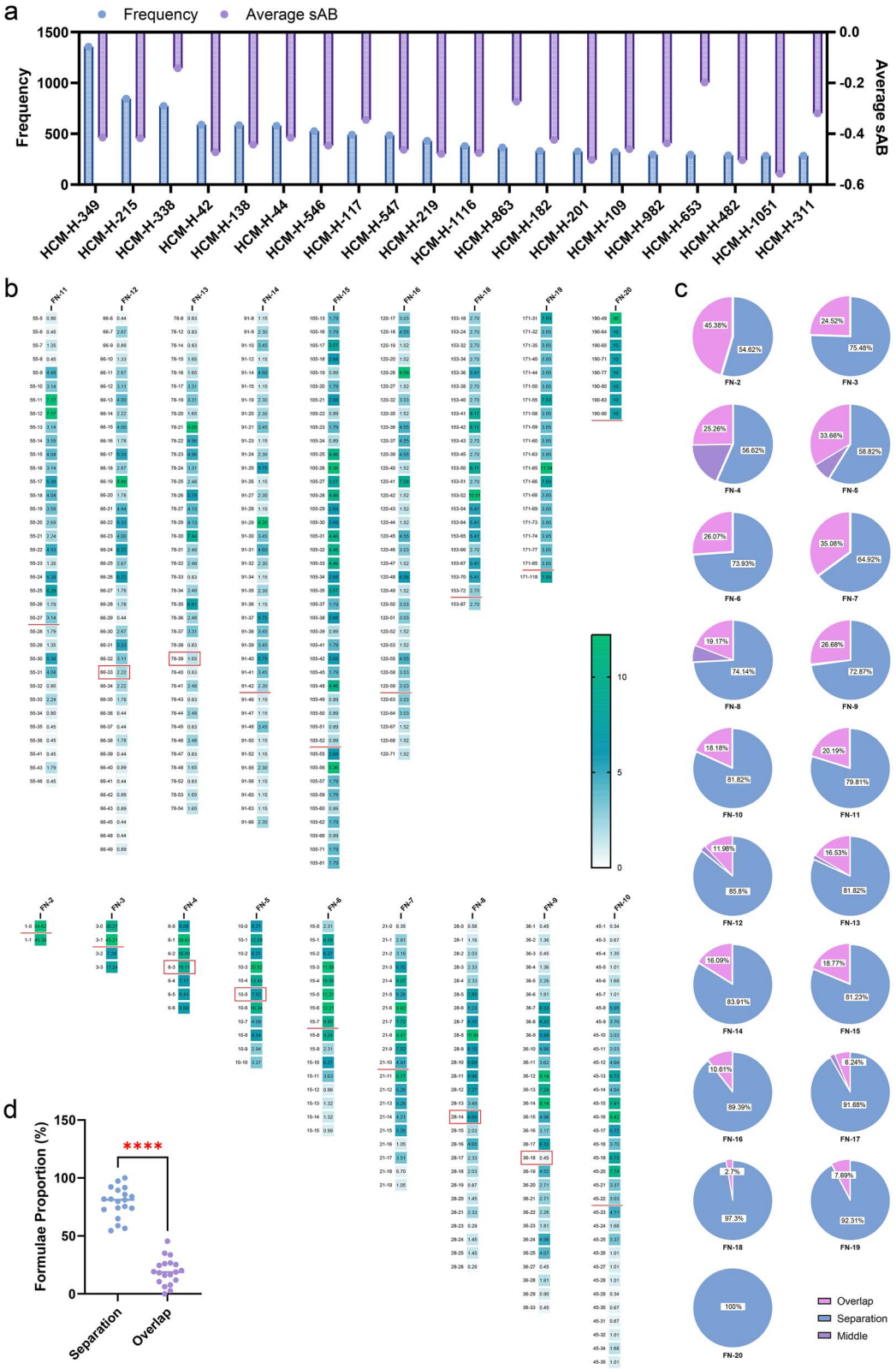

Figure 6. Network module location of classic TCM formulas. (a) The interleaved scatter with bars plots the frequency and average sAB values of the top 20 herbs in classic TCM formulas. (b) The heat map plot of the topological overlap and separation statistics between pairs of herbs in each classic TCM formula; FN−* represents the classic TCM formula that includes * number of herbs; the *x*–*y* value pair indicates that *x* represents the number of herbal pairs in FN−*, while *y* represents the number of herbal pairs exhibiting topological overlap; the colors and numbers within the heat map indicate the proportion of each *x*–*y* type. (c) The pie plot of the proportions of three states (overlap, separation, and middle) of herbal pairs in classic TCM formulas containing varying quantities of herbs. (d) the scatter plot of the proportions of the formulas in the separation state and the formulas in the overlap state. ****P-value < .0001, as determined by the two-tailed paired t-test.

effects. Furthermore, as the number of combined herbs increases, the complexity of their combinations also rises, promoting network topological separation that enhances synergy among the herbs.

Next, we quantified the network-based relationships between the target sets of herbal formulas and diseases, which is a critical aspect of formulation principles. Considering clinical incidence and the breadth of research data on disease targets, we selected CCD (ICD-11-SA60) and RA (ICD-11-FA20) as case studies for formula-disease network analysis (Supplementary Tables S7 and S8). Subsequently, we mapped the distance (dAB value) between the herbs in the formulas and the diseases to a random distribution under identical conditions, calculating the corresponding *Z*-score (Equation (6)) to quantify network proximity (see Methods and Supplementary Table S9). The network distance analysis revealed that most distances between herbs and diseases fell within a range of 2. As the number of herbal targets increased, the distance between the diseases and herbs approached 1, indicating complete proximity (Fig. 7a and b). Specifically, the average distances from CCD and RA to these herbs were 1.75 (average *Z*-score = −3.60) and 1.74 (average *Z*-score = −4.08), respectively (Fig. 7c and d). Further analysis showed that formulas targeting these diseases predominantly contained herbs closely associated with the diseases, with proportions of proximal herbs exceeding 50%–98.90% for CCD and 88.20% for RA (Fig. 7e–h). These findings suggest a robust relationship between diseases and their associated herbs, indicating that the disease target sets are significantly synergistically influenced by the herbs in the formulas, thereby enhancing therapeutic effects.

Building on the topological relationships among herbs, formulas, and diseases, we propose an analysis strategy termed HCM to enhance our understanding and prediction of the synergistic therapeutic mechanisms of TCM formulas. Specifically, when TCM formulas are utilized to treat specific diseases, the herbal–herbal target network is separated to facilitate complementary synergistic effects, while the disease–herbal target sets intersect within the network, thereby emphasizing the direct impact of herbs on diseases.

Case study: network and pharmacological validation of formula YanChuanQin for acute gouty arthritis

To validate the applicability of the HCM, we employed the herbal formula YCQ (Chinese Patent Number: CN 202411051001.9) to evaluate its efficacy in treating AGA. The herbs in YCQ—YHS (HCM-H-1356), CW (HCM-H-136), and QJ (HCM-H-951)—exhibited significant network segregation (sAB values of 0.23, 0.16, and −0.03) and close connections to AGA (Z-score values of −2.31, −4.4, and −8.06) (Fig. 8a). Notably, the similarity analysis of 111 YCQ molecules, which satisfied pharmacokinetic criteria (see Methods), revealed that the average structural similarity was significantly lower than the random distribution at only 0.3623 (*P*-value < .0001), whereas the average similarity in physicochemical properties was high at 0.6866 (*P*-value < .0001) (Supplementary Fig. S6a and b and Supplementary Table S10). Molecular network clustering analysis identified three major clusters associated with YHS, CW, and QJ, containing key molecules listed in the Chinese Pharmacopeia: tetrahydropalmatine (MOL013), gentiopicroside (MOL138), and aconitine (MOL072) (Fig. 8b). Alkaloids were the predominant molecules in YHS and CW (94.92% and 89.74%, respectively), while terpenoids were the primary molecules in QJ (84.62%) (Fig. 8c and Supplementary Fig. S6c). Additionally, the distribution of the targets of YHS and CW exhibited a significant aggregation effect, whereas targets from QJ showed intersections with the other two herbs (Fig. 8d and Supplementary Fig. S6d–f and Supplementary Table S11). These findings indicated that the YCQ formula aligns with HCM and reveals notable differences at both molecular and target levels.

Next, we evaluated the therapeutic effects of the YCQ formula and its index constituent combination (TGA) using an MSU-induced acute gout mouse model (Supplementary Fig. S7a). Analysis of the ASI and TWL indicated significant improvements in the ankle swelling and thermal pain sensitivity of mice in the YCQ and TGA groups compared to the MSU model group (*P*-value < .05) (Fig. 8e–h and Supplementary Fig. S7b). These results suggest that YCQ has a clear efficacy in alleviating AGA symptoms. Furthermore, the systems pharmacology framework was employed to investigate the potential mechanisms associated with the 45 YCQ targets (Supplementary Tables S12 and S13).

Initially, YCQ targets were primarily enriched in tissues such as the liver (degree: 38), skeletal muscle (degree: 32), and whole blood (degree: 30), which engage in critical processes including tissue remodeling, inflammatory response, purine metabolism, and uric acid filtration and excretion during AGA [45–52] (Fig. 9a and Supplementary Fig. S8a). Moreover, GO enrichment analyses revealed that YCQ targets are localized in various cellular compartments (GO:0016323, GO:1904813, GO:0031966, etc.), implicated in processes regulating the inflammatory response, metabolic regulation, and oxidative stress, including the olefinic compound metabolic process (GO:0120254), steroid catabolic process (GO:0006706), response to lipopolysaccharide (GO:0032496), monocarboxylic acid transport (GO:0015718), and response to oxidative stress (GO:0006979) (Fig. 9b). Similarly, KEGG pathway enrichment analysis revealed that YCQ targets influenced various categories of pathways (metabolism, organismal systems, cellular processes, etc.), including the steroid hormone biosynthesis (hsa00140), metabolism of xenobiotics by cytochrome P450 (hsa00980), IL-17 signaling pathway (hsa04657), arachidonic acid metabolism (hsa00590), and relaxin signaling pathway (hsa04926) (Fig. 9c and d and Supplementary Fig. S8b).

Next, we refined the target enrichment analysis to eliminate redundant information and constructed a comprehensive pathway that delineates YCQ's effects in treating AGA. The downstream effects in this pathway indicated that YCQ primarily modulated both anti-inflammatory and pro-inflammatory signaling modules, influencing inflammation, inflammatory cytokines, inflammasome complexes, impaired metabolic function, monocyte attachment and activation, apoptotic injury, and anti-fibrotic processes (Supplementary Fig. S9). The ELISA results demonstrated that YCQ and TGA significantly reduced levels of key inflammatory mediators (IL-1β, IL-6, TNF-α, and IL-18) in the serum and ankle joint tissues of MSU-induced mice (Fig. 9e). And histopathological analysis revealed that YCQ and TGA significantly ameliorated pathological changes and extensive neutrophil infiltration in the ankle joint tissues (Fig. 9f). Collectively, these findings demonstrated that YCQ affects multiple tissue-specific targets, modulating inflammation-related signaling pathways and the release of key inflammatory mediators, thereby significantly enhancing inflammatory responses and mitigating tissue damage in AGA.

Discussion

In recent years, the accumulation of herbal molecular identification data and high-throughput molecular target experimental data has led to exponential growth in herbal databases [53].

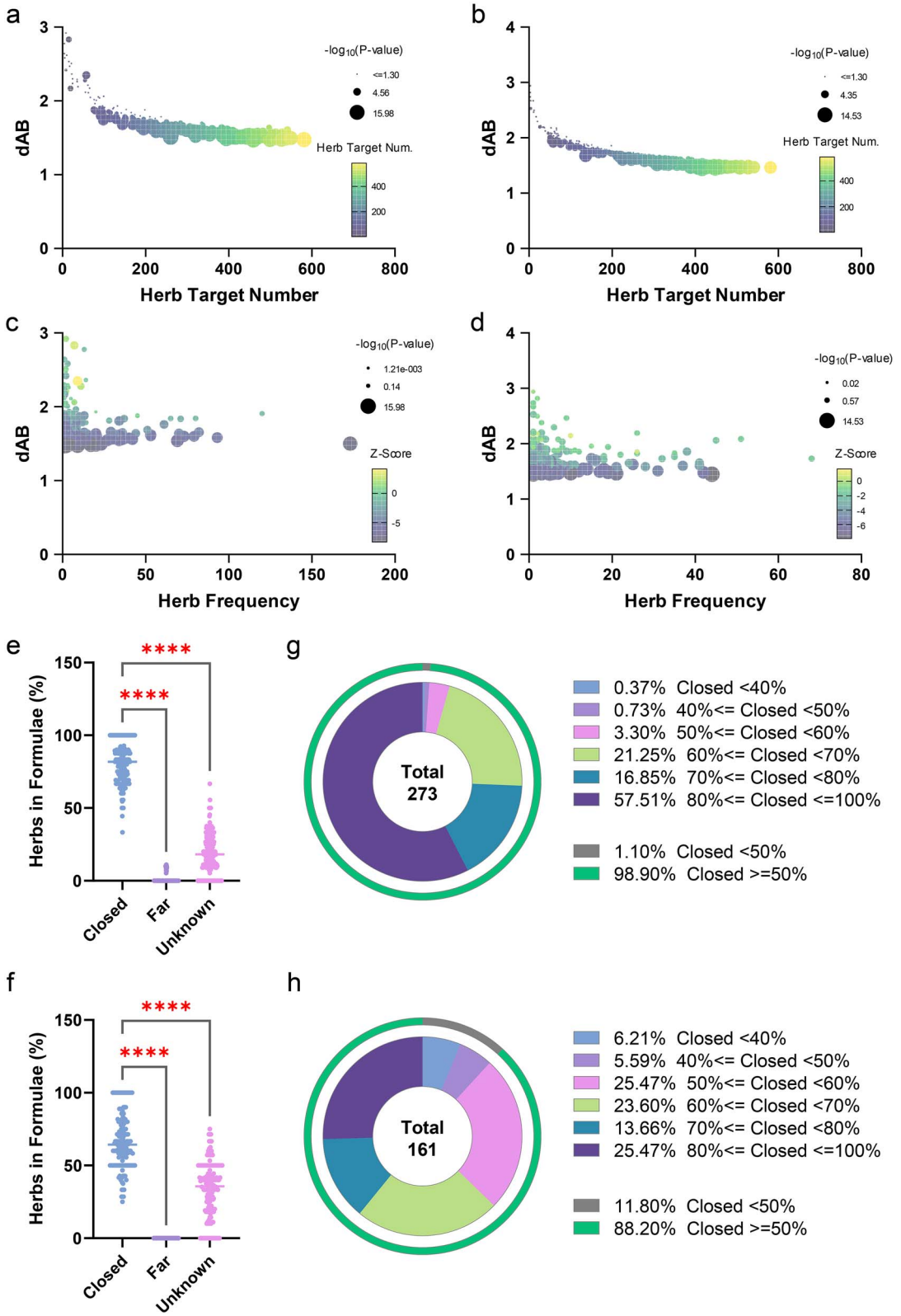

Figure 7. Analysis of the formula-disease network model of CCD and RA. (a and b) The bubble plot of the number of herbal targets and dAB values corresponding to herbs and diseases for the TCM formulas of CCD (a) and RA (b), while the color of each bubble represents the number of herbal targets, and the size of each bubble represents the significance of the dAB value for each herb and disease. (c and d) The bubble plot of the herbal frequency and dAB values for the same TCM formulas, where the color and size of each bubble represent the standard score and the significance of the dAB value for the herbs and diseases, respectively. (e and f) The scatter plot of the proportion of distance state (closed, far, and unknown) of herbs in each TCM formula for the CCD (e) and RA (f). (g and h) The double donut plot of the different proportions of closed distance states of herbs within each TCM formula for CCD (g) and RA (h). ****P-value < .0001, as determined by the ordinary one-way analysis of variance test.

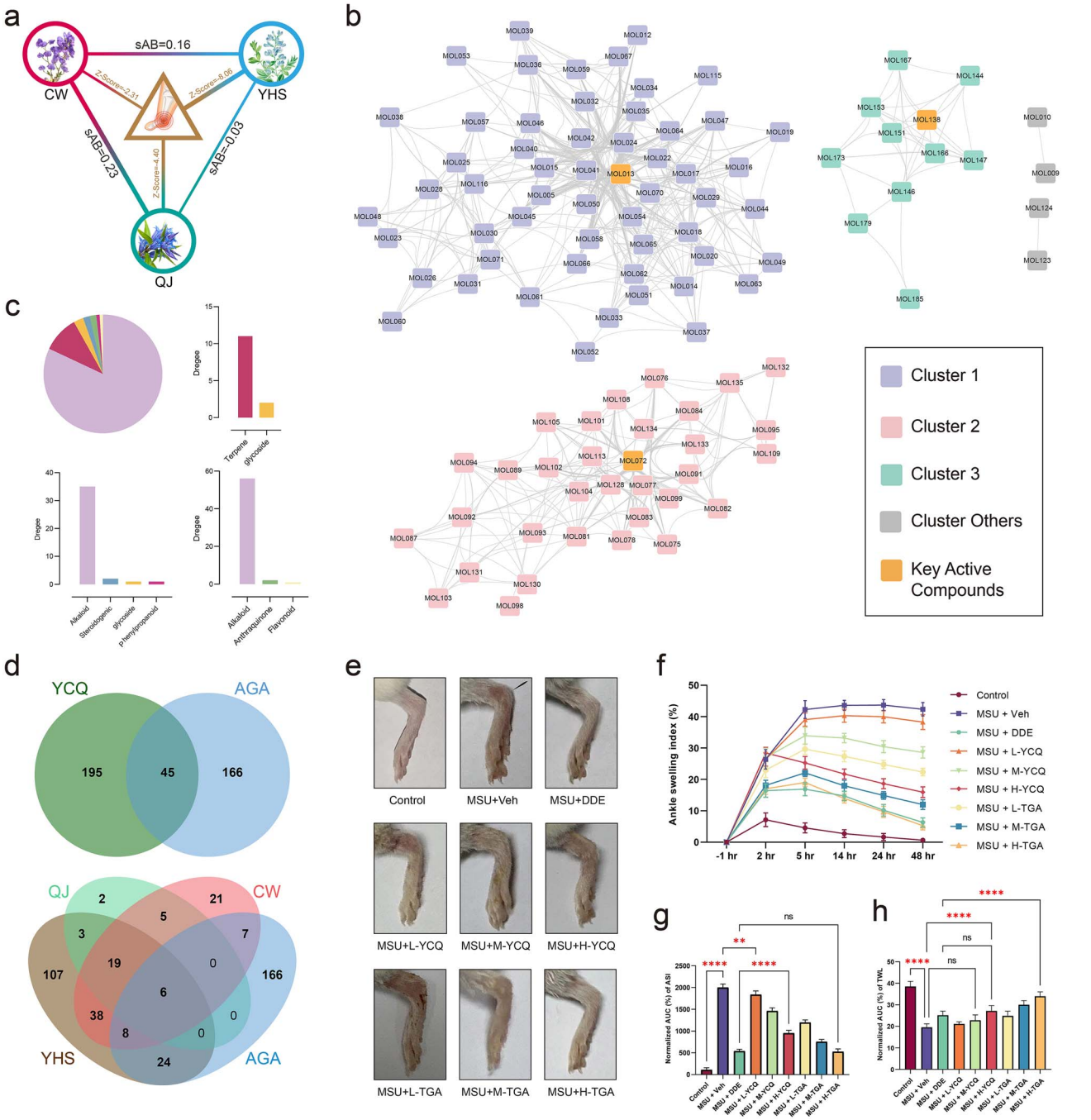

Figure 8. Network pharmacology analysis and in vivo validation of YCQs anti-acute gout arthritis effects. (a) The schematic diagram of a network topology of YCQ and AGA. (b) The network plot of the molecular relationship clustering based on similarities in physicochemical properties. (c) The pie and bar plots of the statistics of molecular structure categories for YCQ and its constituent herbs. (d) The Venn diagram of the number of intersecting targets between YCQ, its herbs, and AGA. (e) the images of the ankle joints of the MSU-induced acute gout mice (24 h after MSU injection), while the black arrow indicates the modeling site. (f) The points and connecting line plot with error bars of the ASI (%) of mice in different groups across varying time points ($n = 6$). (g and h) The bar plot of the normalized area under the curve (%) for the ASI and TWL in different groups ($n = 6$).

This expansion has necessitated advancements in big data analysis methods to keep pace with evolving data landscapes [54, 55]. This study presents a mathematically grounded strategy for the disassembly and prediction of TCM formulas, employing network separation and overlapping strategies to explore the intricate network processes of herbal systems and underlying principles of herbal compatibility. Firstly, the core target screening method aims to tackle the complexities of TCM's multi-molecule and multi-target characteristics. In fact, herbal non-core targets contain more inter-herbal overlapping targets (redundant information), and core targets retain more functionally similar targets (closer proximity on the network). This method, therefore, focuses on reducing the ambiguity in herbal network features caused by informational redundancy. The subsequent network separation and overlap assessment revealed the scale-free biological characteristics of the TCM network that are obscured by redundancy information, confirming its suitability for the contemporary herbal data landscape.

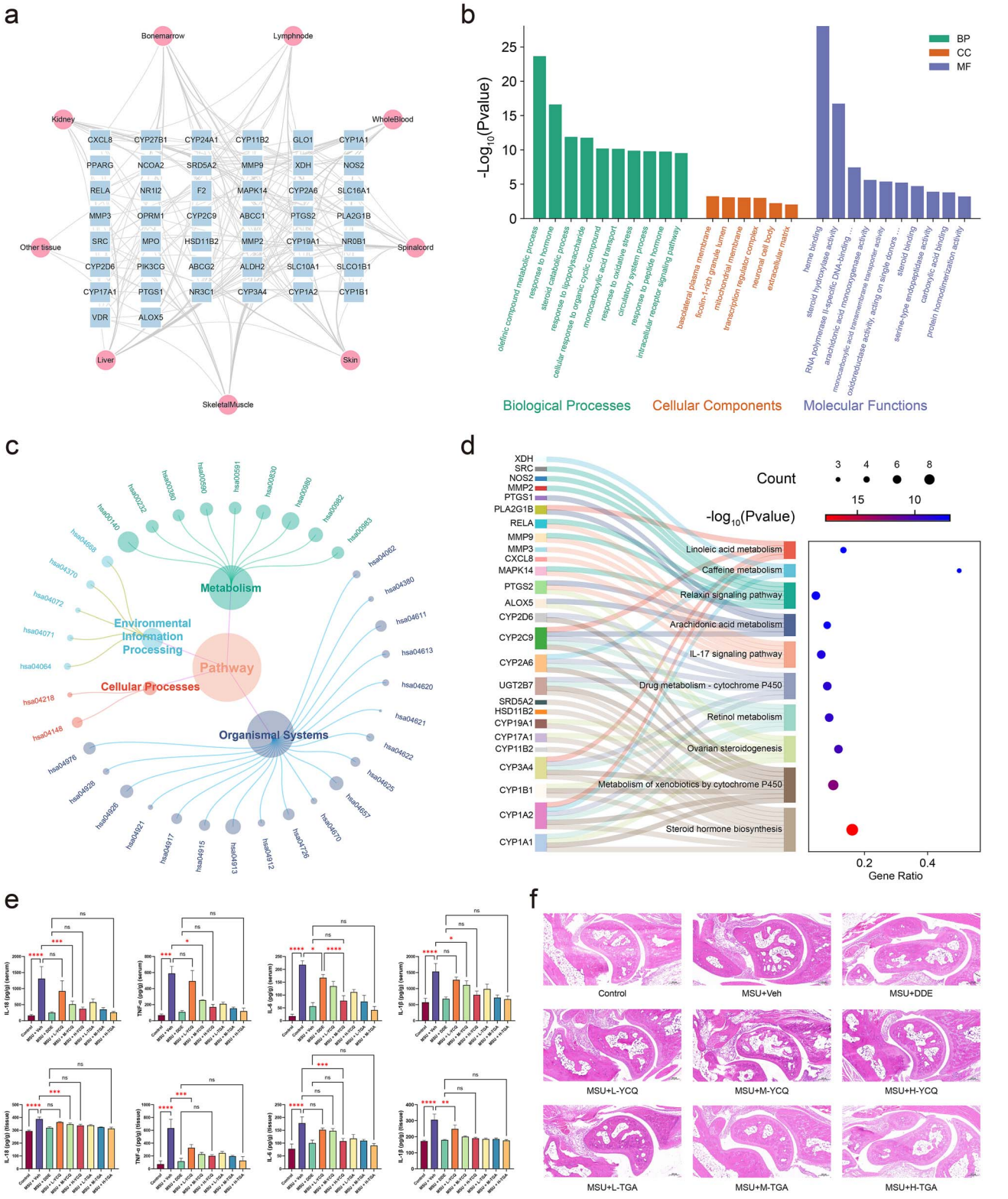

Figure 9. Enrichment analysis and mechanistic validation of YCQ in the treatment of AGA. (a) The network plot of the tissue–target relationships among 45 targets and 9 tissues. (b) The bar plot of GO enrichment analysis results for 45 targets. (c) The circular network plot of the classification information of KEGG-enriched pathways. (d) The Sankey diagram of KEGG enrichment analysis results for 45 targets. (e) The bar plot of the levels of IL-1β, IL-6, TNF-α, and IL-18 in serum and ankle joint tissue from mice in different groups ($n = 3$). (f) Representative micrographs (5×) of ankle joint tissue sections of mice in different groups ($n = 3$). Data are shown as means ± SD, with significance indicated as follows: *P-value < .05, **P-value < .01, ***P-value <.001, ****P-value < .0001, and ns (not significantly different). Statistical significance was determined using the ordinary one-way analysis of variance test.

In the non-redundant network, the network was also able to portray TCM clinically summarized information, indicated by the closer proximity between herbs with similar clinical attributes. Furthermore, while the partially overlapping clinical attributes of the classical herbal pairs led to their closer proximity on the network, we also a considerable degree of separation among the pairs. This indicates that, compared to simple aggregation, herbs tend to favor network separation to achieve synergistic effects. By summarizing the network proximities of classical formulas and specific diseases, two trends were identified: the separation of herbs within TCM formulas and the overlap between herbs and diseases, termed HCM. Subsequently, case studies involving common colds, RA, and AGA exhibited a high consistency between classical therapeutic patterns and this empirical rule, thereby demonstrating the practical applicability of HCM in the rational evaluation and prediction of TCM formulas.

Despite these advancements, this study has limitations. The accuracy of herbal network analysis largely hinges on the comprehensiveness of the TCM database, underscoring the necessity for ongoing enhancement of these resources [56]. Additionally, we observed partial overlap among the herbs in small-scale classic TCM formulas, particularly those with fewer than five herbs. This suggests that the current HCM framework is insufficient in capturing all formulation rules, necessitating further in-depth consideration at both the data level and methodological dimension. For example, the ex vivo and in vivo differences and organ distribution of molecules in TCM formulas may lead to significant alterations in the rules of herbal combinations [57]. The introduction of a TCM pharmacokinetic assessment system, whether through modeling or experimentation, would be a valuable enhancement to the HCM. In addition, the HCM relies more on non-overlapping properties of herbs, with heightened focus on the role of herbal non-core targets in the formulation of combinatorial rules. Meanwhile, more comparative analysis of network distance methods is also a useful addition to the system of HCM [19, 21]. While this research utilized disease data from modern medicine, future investigations could focus more on target information related to TCM symptoms and syndromes, addressing personalized treatment needs and aligning with clinical scenarios [58]. Although network models strive to deconstruct complex rules for herbal combinations, more robust design principles and methods are required to adapt to complex data and clinical requirements.

In summary, this study provides a new paradigm for advancing research on herbal combinations in TCM and preliminarily explores key areas for future investigation that may enhance our understanding and application of TCM.

Key Points

- **Non-redundant network framework application:** This study proposes a multi-network strategy based on core information screening method is proposed to refine herbal target information, in response to the challenge of information redundancy arising from the rapid expansion of traditional Chinese medicine (TCM) data.
- **Clinical information network characterization:** This study investigates the extent of clinical information representation in TCM through an analysis of separation and overlap in a non-redundant network, emphasizing key elements including properties, meridians, and therapeutic classifications.
- **Herbal combination model (HCM) refinement:** This study employs statistical analyses of classical TCM formulas to examine the phenomenon of herbal separation and the overlap between herbs and diseases. These findings contribute to the development of an HCM aimed at enhancing the understanding of TCM interactions.
- **HCM validation of classical TCM formulas:** This study employed statistical analysis of classical TCM formulas for two representative diseases, the common cold and rheumatoid arthritis, to validate the efficacy of the HCM. This validation enhances our understanding of the mechanisms underlying TCM combinations.
- **HCM empirical support of new TCM formula:** In vivo and in vitro experimental studies of the new formula YanChuanQin in acute gouty arthritis have provided substantial evidence for the theoretical framework of HCM, thereby reinforcing its application in complex diseases.

Acknowledgments

The authors thank the anonymous reviewers for their valuable suggestions. This work was supported by the 2021 Shandong Provincial Key RD Program (Major Technological Innovation Project) project (Grant Number 2021CXGC010509), the Key RD Projects of Ningxia Hui Nationality Autonomous Region in 2022 (Grant Number 2022ZDYF0410).

Author contributions

X.T.C. and Y.H.W. conceived the project and strategies. M.J.W. and X.T.C. designed and carried out the experiments, analyzed data, and wrote the manuscript. M.X.L., S.S.Z., and J.G. supervised the work and corrected the manuscript. M.J.W., N.Z., H.Y.L., J.H.W., Y.L., C.W., L.L., and Z.Z.W. were responsible for data collection. M.J.W., H.Y.L., L.Z., H.X.W., and Z.H.G. participated the experimental work on the therapeutic efficacy and corrected the manuscript. All authors read and approved the final manuscript.

Supplementary material

Supplementary material is available at *Briefings in Bioinformatics* online.

Conflict of interest: No competing interest is declared.

Funding

This work was supported by the 2021 Shandong Provincial Key RD Program (Major Technological Innovation Project) project (Grant Number 2021CXGC010509), the Key RD Projects of Ningxia Hui Nationality Autonomous Region in 2022 (Grant Number 2022ZDYF0410).

Data availability

All data supporting the results of this study are available within the paper. And the corresponding data can be accessed through the FigShare platform (https://doi.org/10.6084/m9.figshare.28782539.v2).

References

1. Guo H, Mao H, Pan G. *et al.* Antagonism of cortex Periplocae extract-induced catecholamines secretion by Panax notoginseng saponins in cultured bovine adrenal medullary cells by drug combinations. *J Ethnopharmacol* 2013;**147**:447–55. https://doi.org/10.1016/j.jep.2013.03.036
2. Siddiqui SA, Khan S, Wani SA. Controlling diabetes with the aid of medicinal herbs: a critical compilation of a decade of research. *Crit Rev Food Sci Nutr* 2023;**63**:12552–66. https://doi.org/10.1080/10408398.2022.2103088
3. Song Z, Chen G, Chen CY. AI empowering traditional Chinese medicine? *Chem Sci* 2024;**15**:16844–86. https://doi.org/10.1039/D4SC04107K
4. Ren Z, Ren Y, Li Z. *et al.* TCMM: a unified database for traditional Chinese medicine modernization and therapeutic innovations. *Comput Struct Biotechnol J* 2024;**23**:1619–30. https://doi.org/10.1016/j.csbj.2024.04.016
5. Yang HY, Liu ML, Luo P. *et al.* Network pharmacology provides a systematic approach to understanding the treatment of ischemic heart diseases with traditional Chinese medicine. *Phytomedicine* 2022;**104**:154268. https://doi.org/10.1016/j.phymed.2022.154268
6. Luo S, Huang M, Lu X. *et al.* Optimized therapeutic potential of Yinchenhao decoction for cholestatic hepatitis by combined network meta-analysis and network pharmacology. *Phytomedicine* 2024;**129**:155573. https://doi.org/10.1016/j.phymed.2024.155573
7. Park M, Baek SJ, Park SM. *et al.* Comparative study of the mechanism of natural compounds with similar structures using docking and transcriptome data for improving in silico herbal medicine experimentations. *Brief Bioinform* 2023;**24**:24. https://doi.org/10.1093/bib/bbad344
8. Ru J, Li P, Wang J. *et al.* TCMSP: a database of systems pharmacology for drug discovery from herbal medicines. *J Chem* 2014;**6**:13. https://doi.org/10.1186/1758-2946-6-13
9. Xue R, Fang Z, Zhang M. *et al.* TCMID: traditional Chinese medicine integrative database for herb molecular mechanism analysis. *Nucleic Acids Res* 2013;**41**:D1089–95. https://doi.org/10.1093/nar/gks1100
10. Springer L, Gohlke BO, Goede A. *et al.* SuperTCM: a biocultural database combining biological pathways and historical linguistic data of Chinese Materia Medica for drug development. *Biomedicine & Pharmacotherapy = Biomedecine & Pharmacotherapie* 2021;**144**:112315. https://doi.org/10.1016/j.biopha.2021.112315
11. Yu H, Chen J, Xu X. *et al.* A systematic prediction of multiple drug-target interactions from chemical, genomic, and pharmacological data. *PloS One* 2012;**7**:e37608. https://doi.org/10.1371/journal.pone.0037608
12. Zheng C, Guo Z, Huang C. *et al.* Large-scale direct targeting for drug repositioning and discovery. *Sci Rep* 2015;**5**:11970. https://doi.org/10.1038/srep11970
13. Zdrazil B, Felix E, Hunter F. *et al.* The ChEMBL database in 2023: a drug discovery platform spanning multiple bioactivity data types and time periods. *Nucleic Acids Res* 2024;**52**:D1180–92. https://doi.org/10.1093/nar/gkad1004
14. Grissa D, Junge A, Tudor O I. *et al.* Diseases 2.0: a weekly updated database of disease-gene associations from text mining and data integration. *Database: the journal of biological databases and curation* 2022;**2022**:baac019. https://doi.org/10.1093/database/baac019
15. Knox C, Wilson M, Klinger CM. *et al.* DrugBank 6.0: the DrugBank knowledgebase for 2024. *Nucleic Acids Res* 2024;**52**:D1265–75. https://doi.org/10.1093/nar/gkad976
16. Piñero J, Ramírez-Anguita JM. *et al.* The DisGeNET knowledge platform for disease genomics: 2019 update. *Nucleic Acids Res* 2020;**48**:D845–55. https://doi.org/10.1093/nar/gkz1021
17. Stelzer G, Rosen N, Plaschkes I. *et al.* The GeneCards suite: from gene data mining to disease genome sequence analyses. *Curr Protoc Bioinformatics* 2016;**54**:1.30.31–31.30.33. https://doi.org/10.1002/cpbi.5
18. Hamosh A, Amberger JS, Bocchini C. *et al.* Online Mendelian inheritance in man (OMIM®): victor McKusick's magnum opus. *Am J Med Genet A* 2021;**185**:3259–65. https://doi.org/10.1002/ajmg.a.62407
19. Cheng F, Kovács IA, Barabási A-L. Network-based prediction of drug combinations. *Nat Commun* 2019;**10**:1197. https://doi.org/10.1038/s41467-019-09186-x
20. Das J, Yu H. HINT: high-quality protein interactomes and their applications in understanding human disease. *BMC Syst Biol* 2012;**6**:92. https://doi.org/10.1186/1752-0509-6-92
21. Wang Y, Yang H, Chen L. *et al.* Network-based modeling of herb combinations in traditional Chinese medicine. *Brief Bioinform* 2021;**22**:bbab106. https://doi.org/10.1093/bib/bbab106
22. Ye X, Wu J, Zhang D. *et al.* How Aconiti radix Cocta can treat gouty arthritis based on systematic pharmacology and UPLC-QTOF-MS/MS. *Front Pharmacol* 2021;**12**:618844. https://doi.org/10.3389/fphar.2021.618844
23. Chan KH, Ching JYL, Chan KL. *et al.* Therapeutic effect of Duhuo Jisheng decoction add-on Tui-na manipulation on osteoarthritis of knee: a randomized controlled trial. *Chinese Medicine* 2023;**18**:82. https://doi.org/10.1186/s13020-023-00737-5
24. Doak Bradley C, Over B, Giordanetto F. *et al.* Oral Druggable space beyond the rule of 5: insights from drugs and clinical candidates. *Chem Biol* 2014;**21**:1115–42. https://doi.org/10.1016/j.chembiol.2014.08.013
25. Wu C, Orozco C, Boyer J. *et al.* BioGPS: an extensible and customizable portal for querying and organizing gene annotation resources. *Genome Biol* 2009;**10**:R130. https://doi.org/10.1186/gb-2009-10-11-r130
26. Zhou Y, Zhou B, Pache L. *et al.* Metascape provides a biologist-oriented resource for the analysis of systems-level datasets. *Nat Commun* 2019;**10**:1523. https://doi.org/10.1038/s41467-019-09234-6
27. Shannon P, Markiel A, Ozier O. *et al.* Cytoscape: a software environment for integrated models of biomolecular interaction networks. *Genome Res* 2003;**13**:2498–504. https://doi.org/10.1101/gr.1239303
28. Broido AD, Clauset A. Scale-free networks are rare. *Nat Commun* 2019;**10**:1017. https://doi.org/10.1038/s41467-019-08746-5
29. Song M, Cui M, Fang Z. *et al.* Advanced research on extracellular vesicles based oral drug delivery systems. *J Control Release* 2022;**351**:560–72. https://doi.org/10.1016/j.jconrel.2022.09.043
30. Berillo D, Zharkinbekov Z, Kim Y. *et al.* Stimuli-responsive polymers for transdermal, transmucosal and ocular drug delivery. *Pharmaceutics* 2021;**13**. https://doi.org/10.3390/pharmaceutics13122050
31. Cai T, Wang X, Li B. *et al.* Deciphering the synergistic network regulation of active components from SiNiSan against irritable bowel syndrome via a comprehensive strategy: combined effects of synephrine, paeoniflorin and naringin. *Phytomedicine* 2021;**86**:153527. https://doi.org/10.1016/j.phymed.2021.153527
32. Guan X, Zheng X, Vong CT. *et al.* Combined effects of berberine and evodiamine on colorectal cancer cells and cardiomyocytes in vitro. *Eur J Pharmacol* 2020;**875**:173031. https://doi.org/10.1016/j.ejphar.2020.173031

33. Song J, Xu X, He S. *et al.* Identification of the therapeutic effect and molecular mechanism of *Coptis chinensis* Franch. and Magnolia officinalis var. biloba on chronic gastritis. *J Ethnopharmacol* 2023;**317**:116864. https://doi.org/10.1016/j.jep.2023.116864
34. Jin TY, Rong PQ, Liang HY. *et al.* Clinical and preclinical systematic review of Panax ginseng C.A. Mey and its compounds for fatigue. *Front Pharmacol* 2020;**11**:1031. https://doi.org/10.3389/fphar.2020.01031
35. Shen X, Wu Y, Chen P. *et al.* Anti-platelet aggregation activities of different grades of *Angelica sinensis* and their therapeutic mechanisms in rats with blood deficiency: insights from metabolomics and lipidomics analyses. *Front Pharmacol* 2023;**14**:1230861. https://doi.org/10.3389/fphar.2023.1230861
36. Bai J, Qi J, Yang L. *et al.* A comprehensive review on ethnopharmacological, phytochemical, pharmacological and toxicological evaluation, and quality control of *Pinellia ternata* (Thunb.) Breit. *J Ethnopharmacol* 2022;**298**:115650. https://doi.org/10.1016/j.jep.2022.115650
37. Liu YX, Song XM, Dan LW. *et al.* Astragali radix: comprehensive review of its botany, phytochemistry, pharmacology and clinical application. *Arch Pharm Res* 2024;**47**:165–218. https://doi.org/10.1007/s12272-024-01489-y
38. Qi Y, Ni S, Heng X. *et al.* Uncovering the potential mechanisms of *Coptis chinensis* Franch. For serious mental illness by network pharmacology and pharmacology-based analysis. *Drug Des Devel Ther* 2022;**16**:325–42. https://doi.org/10.2147/DDDT.S342028
39. Yao J, Liu J, He Y. *et al.* Systems pharmacology reveals the mechanism of Astragaloside IV in improving immune activity on cyclophosphamide-induced immunosuppressed mice. *J Ethnopharmacol* 2023;**313**:116533. https://doi.org/10.1016/j.jep.2023.116533
40. Shi L, Luo J, Wei X. *et al.* The protective role of ginsenoside Rg3 in heart diseases and mental disorders. *Front Pharmacol* 2024;**15**:1327033. https://doi.org/10.3389/fphar.2024.1327033
41. Guo W, Wang W, Lei F. *et al.* Angelica sinensis polysaccharide combined with cisplatin reverses cisplatin resistance of ovarian cancer by inducing ferroptosis via regulating GPX4. *Biomed Pharmacother* 2024;**175**:116680. https://doi.org/10.1016/j.biopha.2024.116680
42. Zhao W, Duan C, Liu Y. *et al.* Modulating effects of Astragalus polysaccharide on immune disorders via gut microbiota and the TLR4/NF-κB pathway in rats with syndrome of dampness stagnancy due to spleen deficiency. *J Zhejiang Univ Sci B* 2023;**24**:650–62. https://doi.org/10.1631/jzus.B2200491
43. Ding Y, Brand E, Wang W. *et al.* Licorice: resources, applications in ancient and modern times. *J Ethnopharmacol* 2022;**298**:115594. https://doi.org/10.1016/j.jep.2022.115594
44. Kim DH, Kim JS, Kim J. *et al.* Therapeutic effects of Licorice and dried ginger decoction on activity-based anorexia in BALB/c AnNCrl mice. *Front Pharmacol* 2020;**11**:594706. https://doi.org/10.3389/fphar.2020.594706
45. Yang F, Men R, Lv L. *et al.* Engaging natural regulatory myeloid cells to restrict T-cell hyperactivation-induced liver inflammation via extracellular vesicle-mediated purine metabolism regulation. *Theranostics* 2024;**14**:4874–93. https://doi.org/10.7150/thno.97427
46. Jheng JR, Bai Y, Noda K. *et al.* Skeletal muscle SIRT3 deficiency contributes to pulmonary vascular remodeling in pulmonary hypertension due to heart failure with preserved ejection fraction. *Circulation* 2024;**150**:867–83. https://doi.org/10.1161/CIRCULATIONAHA.124.068624
47. Blankestijn JM, Baalbaki N, Bazdar S. *et al.* Whole blood transcriptome in long-COVID patients reveals association with lung function and immune response. *J Allergy Clin Immunol* 2024;**154**:807–18. https://doi.org/10.1016/j.jaci.2024.04.032
48. Mitroulis I, Hajishengallis G, Chavakis T. Bone marrow inflammatory memory in cardiometabolic disease and inflammatory comorbidities. *Cardiovasc Res* 2024;**119**:2801–12. https://doi.org/10.1093/cvr/cvad003
49. Gao X, Han Z, Huang C. *et al.* An anti-inflammatory and neuroprotective biomimetic nanoplatform for repairing spinal cord injury. *Bioact Mater* 2022;**18**:569–82. https://doi.org/10.1016/j.bioactmat.2022.05.026
50. Suijk DLS, van Baar MJB, van Bommel EJM. *et al.* SGLT2 inhibition and uric acid excretion in patients with type 2 diabetes and Normal kidney function. *Clin J Am Soc Nephrol* 2022;**17**:663–71. https://doi.org/10.2215/CJN.11480821
51. Fassett MS, Braz JM, Castellanos CA. *et al.* IL-31-dependent neurogenic inflammation restrains cutaneous type 2 immune response in allergic dermatitis. *Sci Immunol* 2023;**8**:eabi6887. https://doi.org/10.1126/sciimmunol.abi6887
52. Grenier P, Chénard V, Bertrand N. The mechanisms of anti-PEG immune response are different in the spleen and the lymph nodes. *J Control Release* 2023;**353**:611–20. https://doi.org/10.1016/j.jconrel.2022.12.005
53. Yan D, Zheng G, Wang C. *et al.* HIT 2.0: an enhanced platform for herbal ingredients' targets. *Nucleic Acids Res* 2022;**50**:D1238–43. https://doi.org/10.1093/nar/gkab1011
54. Danishuddin KS, Kim JJ. Spatial transcriptomics data and analytical methods: an updated perspective. *Drug Discov Today* 2024;**29**:103889. https://doi.org/10.1016/j.drudis.2024.103889
55. Liu X, Gong X, Liu Y. *et al.* Application of high-throughput sequencing on the Chinese herbal medicine for the data-mining of the bioactive compounds. *Front Plant Sci* 2022;**13**:900035. https://doi.org/10.3389/fpls.2022.900035
56. Niu Q, Li H, Tong L. *et al.* TCMFP: a novel herbal formula prediction method based on network target's score integrated with semi-supervised learning genetic algorithms. *Brief Bioinform* 2023;**24**:bbad102. https://doi.org/10.1093/bib/bbad102
57. Zhou M, Hong Y, Lin X. *et al.* Recent pharmaceutical evidence on the compatibility rationality of traditional Chinese medicine. *J Ethnopharmacol* 2017;**206**:363–75. https://doi.org/10.1016/j.jep.2017.06.007
58. Wu Y, Zhang F, Yang K. *et al.* SymMap: an integrative database of traditional Chinese medicine enhanced by symptom mapping. *Nucleic Acids Res* 2019;**47**:D1110–7. https://doi.org/10.1093/nar/gky1021

Briefings in Bioinformatics, 2025, **26(3)**, bbaf229
https://doi.org/10.1093/bib/bbaf229
Case Study